eprints@whiterose.ac.uk
https://eprints.whiterose.ac.uk/

Article

Examining the Relationship between Semiquantitative Methods Analysing Concentration-Time and Enhancement-Time Curves from Dynamic-Contrast Enhanced Magnetic Resonance Imaging and Cerebrovascular Dysfunction in Small Vessel Disease [†]

Jose Bernal [1,*] , **María Valdés-Hernández** [1,*] , **Javier Escudero** [2] , **Eleni Sakka** [1] ,
Paul A. Armitage [3] , **Stephen Makin** [4] , **Rhian M. Touyz** [4] and **Joanna M. Wardlaw** [1]

[1] Centre for Clinical Brain Sciences, University of Edinburgh, Edinburgh EH16 4SB, UK;
eleni.sakka@ed.ac.uk (E.S.); Joanna.Wardlaw@ed.ac.uk (J.M.W.)

[2] School of Engineering, University of Edinburgh, Edinburgh EH9 3FB, UK; javier.escudero@ed.ac.uk

[3] Academic Unit of Radiology, University of Sheffield, Sheffield S10 2JF, UK; p.armitage@sheffield.ac.uk

[4] Institute of Cardiovascular and Medical Sciences, University of Glasgow, Glasgow G12 8TA, UK;
Stephen.Makin@glasgow.ac.uk (S.M.); Rhian.Touyz@glasgow.ac.uk (R.M.T.)

[*] Correspondence: jose.bernal@ed.ac.uk (J.B.); m.valdes-hernan@ed.ac.uk (M.V.-H.)

[†] This paper is an extended version of our paper published in: Bernal, J., Valdés-Hernández, M.d.C.,
Escudero, J., Armitage, P.A., Makin, S., Touyz, R.M., and Wardlaw, J.W. Analysis of spatial spectral features
of dynamic contrast-enhanced brain magnetic resonance images for studying small vessel disease.
In: Zheng Y., Williams B., Chen K. (eds) Medical Image Understanding and Analysis. MIUA 2019.
Communications in Computer and Information Science, vol 1065. Springer: Cham, Switzerland, 2019;
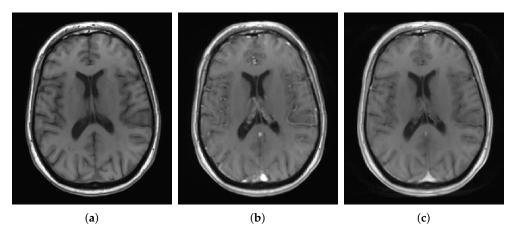pp. 282–293.

check for
updates

Abstract: Dynamic contrast-enhanced magnetic resonance imaging (DCE-MRI) can be used to examine the distribution of an intravenous contrast agent within the brain. Computational methods have been devised to analyse the contrast uptake/washout over time as reflections of cerebrovascular dysfunction. However, there have been few direct comparisons of their relative strengths and weaknesses. In this paper, we compare five semiquantitative methods comprising the slope and area under the enhancement-time curve, the slope and area under the concentration-time curve ($Slope_{Con}$ and AUC_{Con}), and changes in the power spectrum over time. We studied them in cerebrospinal fluid, normal tissues, stroke lesions, and white matter hyperintensities (WMH) using DCE-MRI scans from a cohort of patients with small vessel disease (SVD) who presented mild stroke. The total SVD score was associated with AUC_{Con} in WMH ($p < 0.05$), but not with the other four methods. In WMH, we found higher AUC_{Con} was associated with younger age ($p < 0.001$) and fewer WMH ($p < 0.001$), whereas $Slope_{Con}$ increased with younger age ($p > 0.05$) and WMH burden ($p > 0.05$). Our results show the potential of different measures extracted from concentration-time curves extracted from the same DCE examination to demonstrate cerebrovascular dysfunction better than those extracted from enhancement-time curves.

Keywords: cerebrovascular alteration descriptors; small vessel disease; dynamic contrast-enhanced magnetic resonance imaging

1. Introduction

Dynamic contrast-enhanced magnetic resonance imaging (DCE-MRI) in the brain is typically considered for examining the integrity of grey and white matter and potential contrast leakage into cerebrospinal fluid (CSF) cavities [1–3]. In this imaging modality, a series of MRI scans are taken before and after intravenous Gadolinium-based contrast agent administration to image signal-time trajectories of both healthy and pathological brain regions, as illustrated in Figure 1. Such trajectories may vary depending on the capillary density and the disruption of the blood–brain barrier or blood–CSF barrier, among other factors. Therefore, their precise analysis may help to understand better the mechanisms behind pathological cerebrovascular processes.

(a)	(b)	(c)

Figure 1. Dynamic contrast-enhanced magnetic resonance imaging acquisition. From left to right, axial slices of T1-w scans before, 1 min after, and 24 min after intravenous Gadolinium-based contrast agent injection, respectively. (**a**) Before contrast, (**b**) 1 min after, (**c**) 24 min after.
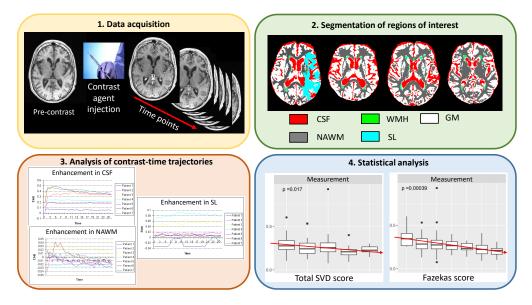
Computational approximations for studying signal-time trajectories are classified into two groups: semiquantitative and quantitative [3]. The former group of methods does not make any assumptions about the distribution of contrast agent within the brain, i.e., are model free. Methods that fall under this category analyse the area under the enhancement curve [4], signal enhancement slope [5,6], and dynamic spectral and texture features [7,8]. The latter group of methods describes signal-time curves as a result of interactions between cerebral capillaries and the extracellular extravascular space through pharmacokinetic modelling. The approximation consists of estimating unknown model parameter values from the input data through regression. However, factors such as scanner signal drift, tissue variations, and imaging artefacts introduce systematic errors hampering quantitative assessments [3,9–11].

In this work, we study to what extent semiquantitative methods analysing signal-time trajectories from the same imaging acquisitions reflect cerebrovascular dysfunction. In particular, we examine the strength of their association with clinical parameters: the higher the percentage of variance explained by clinical variables, the more the relevant information the measurement captures. The considered methods are (1) the area under the enhancement-time curve, (2) the slope of the enhancement-time curve, (3) the area under the concentration-time curve, (4) the slope of the concentration-time curve, and (5) the radial power spectrum of the concentration-time curve. We use data from a relatively large cohort ($n = 201$) of patients who had a mild stroke and present a varied range of small vessel disease (SVD) features. The main finding of our work is that the analysis of concentration-time curves reflect key aspects of cerebrovascular dysfunction better than enhancement-time curves.

2. Materials and Methods

The processing pipeline consists of four steps, as illustrated in Figure 2. First, we acquire structural and dynamic scans for each patient in the cohort. Second, we segment all regions of

interest. Third, we analyse contrast-time trajectories in each region. Fourth, we use ANOVA and multiple linear regression to establish whether measurements of contrast uptake/washout vary with any of the clinical variables. Further details of each step are provided in the following sections.

Figure 2. High level schematic of our processing pipeline. First, we acquire dynamic contrast-enhanced scans for each patient. Second, we segment regions of interest into cerebrospinal fluid, grey matter, normal-appearing white matter, white matter hyperintensities, and stroke lesions. Third, we analyse contrast-time trajectories using different approaches: slopes and areas under the enhancement-time and concentration-time curves and changes over time in the radial power spectrum. Fourth, we use ANOVA and multiple linear regression to examine the effect of the burden of white matter hyperintensities (Fazekas score) and all neuroimaging features of small vessel disease (Total SVD score). In Step 4, data points located outside of the whiskers of each boxplot correspond to outliers. CSF: cerebrospinal fluid. WMH: white matter hyperintensity. NAWM: normal-appearing white matter. GM: grey matter. SL: stroke lesion.

2.1. Subjects, Imaging, and Clinical Variables

We used DCE-MRI and clinical data from 201 mild stroke patients with various extents of neuroimaging features of SVD [12,13]. The study was approved by the Lothian Ethics of Medical Research Committee (REC 09/81101/54) and the NHS Lothian R+D Office (2009/W/NEU/14), and all patients gave written informed consent. DCE-MRI scans were obtained approximately a month after stroke presentation using a 3D T1-w spoiled gradient echo sequence (TR/TE = 8.24/3.1 ms, 12° flip angle, 24 cm × 24 cm FoV, 0.9375 mm × 1.25 mm × 4 mm acquired resolution). Following a pre-contrast scan, patients were scanned after an intravenous bolus injection of 0.1mmol/kg of gadoterate meglumine (Gd-DOTA, Dotarem, Guerbet, France) every 73 s during 25 min (leading to 21 frames). We considered age, biological sex (60% male, 40% female), smoker (ever smoker 65% vs. never smoker 35%), diabetes (yes 12% vs. no 88%), hyperlipidaemia (yes 60% vs. no 40%), mean arterial pressure, the total Fazekas score [14] (0–3%, 1–8%, 2–37%, 3–11%, 4–15%, 5–10%, and 6–16%) and the total SVD score [15] (0–33%, 1–24%, 2–23%, 3–13%, and 4–7%).

2.2. Segmentation of Regions of Interest

We examined five regions of interest comprising cerebrospinal fluid, deep grey matter, normal-appearing white matter, WMH, and stroke lesions. To obtain their segment masks, we followed the protocol described in [12], i.e., initial segmentation using validated methods, manual edit by trained analysts, and mask erosion to avoid partial volume [11]. Analysts carried out the rectification process blinded to any other imaging and patient information. Details regarding the validation of the segmentation method and inter-analyst agreement can be found in [7,11,12,16].

2.3. Methods

2.3.1. Methods Analysing the Enhancement-Time Trajectory

Let $S[t] \in \mathbb{R}$, $t \in \{0, ..., T-1\}$ be the measured signal over time, where $S[0]$ represents the signal value before intravenous contrast injection and T the number of time points. Methods analysing the enhancement-time trajectory examine relative signal changes before and after contrast, i.e., $(S[t] - S[0])/S[0]$. We estimated the area under the enhancement-time curve,

$$AUC_{Enh} = \sum_{t=0}^{T-1} \frac{S[t] - S[0]}{S[0]},$$ (1)

and its slope,

$$Slope_{Enh} = \frac{(T-t^*) \cdot \sum_{t=t^*}^{T-1} t \cdot S[t] - \sum_{t=t^*}^{T-1} t \cdot \sum_{t=t^*}^{T-1} S[t]}{(T-t^*) \cdot \sum_{t=t^*}^{T-1} t^2 - (\sum_{t=t^*}^{T-1} t)^2},$$ (2)

where t^* is the time point from where the signal trend is assumed linear. Note that the formulation of the slope permits avoiding the peak of bolus arrival. In our case, we set $t^* = 4$ after visual inspection of all cases in the cohort.

2.3.2. Methods Analysing the Concentration-Time Trajectory

Signal information and imaging parameters can be used to approximate the contrast agent concentration [in millimoles] in time in each region of interest [9]. For that, we converted signal-time curves to concentration-time curves by finding, $c[t]$, that minimises the following expression

$$\min_{c[t]} \left\| \frac{S[t] - S[0]}{S[0]} - e^{-r_2 c[t] TE} \frac{1 - e^{-P-Q[t]} - \cos(\theta_{FA})\left(e^{-P} - e^{-2P-Q[t]}\right)}{1 - e^{-P} - \cos(\theta_{FA})\left(e^{-P-Q[t]} - e^{-2P-Q[t]}\right)} \right\|_2^2,$$ (3)

where $P = TR/T1[0]$, $Q[t] = r_1 \cdot c[t] \cdot TR$; $r_1 = 4.2 s^{-1} mM^{-1}$, $r_2 = 6.7 s^{-1} mM^{-1}$ are the Gadolinium-based contrast agent relaxivities; $TR = 8.24$ ms and $TE = 3.1$ ms are the repetition and echo times; $\theta_{FA} = 12°$ the flip angle; and $T1[t]$ and $T2[t]$ the longitudinal and transversal relaxation times at time t, estimated as described in [9]. The relaxation time is assumed to decrease with contrast agent concentration and relaxivities, $1/Ti[t] = 1/Ti[0] + r_i \cdot c[t]$, $i = 1, 2$. After obtaining the curves, we estimated the area under the concentration-time curve,

$$AUC_{Con} = \sum_{t=0}^{T-1} c[t],$$ (4)

and its slope,

$$Slope_{Con} = \frac{(T-t^*) \cdot \sum_{t=t^*}^{T-1} t \cdot c[t] - \sum_{t=t^*}^{T-1} t \cdot \sum_{t=t^*}^{T-1} c[t]}{(T-t^*) \cdot \sum_{t=t^*}^{T-1} t^2 - (\sum_{t=t^*}^{T-1} t)^2}.$$ (5)

2.3.3. Methods to Analyse Changes in the Radial Power Spectrum

The analysis of the radial power spectrum (RPS) permits scrutinising alterations in the spatial frequency domain due to the intravenous injection of the contrast agent [17]. Similar to previous works in the field [7,8], we computed the RPS for each region of interest and each time point after the peak of bolus arrival by calculating the magnitude spectra and averaging it over all frequencies in concentric rings of width one, as follows

$$R[s; t] = \frac{1}{K} \sum_{k=1}^{K} \frac{1}{2\pi} \int_0^{2\pi} |F_k(s \cos(\theta), s \sin(\theta), t)| \, d\theta,$$ (6)

where F_k denotes the 2D discrete Fourier transform of the k-th axial slice of the input volume, $K = 42$ the number of slices, and $s = \text{round}\left(\sqrt{u^2 + v^2}\right)$ and $\theta = \tan^{-1}(v/u)$ are polar coordinates.

To analyse these signals that include 201 patients $\times$ 129 rings $\times$ 17 time points, we opted for reducing their cardinality to only a set of measurements per patient. We achieved this by reducing it in the direction of the rings and time using the multivariate functional principal component analysis proposed by Happ & Greven [18]. Let $R_p[s;t]$ be the RPS over time of patient $p \in [1, 201]$, $s \in [0, 128]$, $t \in [4, 20]$, the overall process consists of four steps. First, we centred each variable by subtracting its mean value across patients. Second, we computed E eigenfunctions $\Phi_k[s;t]$ and corresponding scores $\xi_{pk}[s]$ by maximising $\sum_p \xi_{pk}[s]^2$, where

$$\xi_{pk}[s] = \sum_{t=t^*}^{T-1} \Phi_k[s;t] \cdot R_p[s;t], \tag{7}$$

subject to $||\Phi_k[s]||^2 = 1$. We set $E = 5$ as the resulting eigenfunctions explained 99% of the data variance. Third, all of these scores $\xi_{pk}[s]$ were arranged in a matrix form, $\Xi \in \mathbb{R}^{201 \times 129 \times E}$, such that the pth row contained $(\xi_{p1}[0], ..., \xi_{p1}[128], ..., \xi_{p5}[0], ..., \xi_{p5}[128])$. Fourth, we calculated principal component scores by means of eigenanalysis on the covariance matrix of Ξ. We considered only the first mode of variation since it explained around the 98% of the data variance.

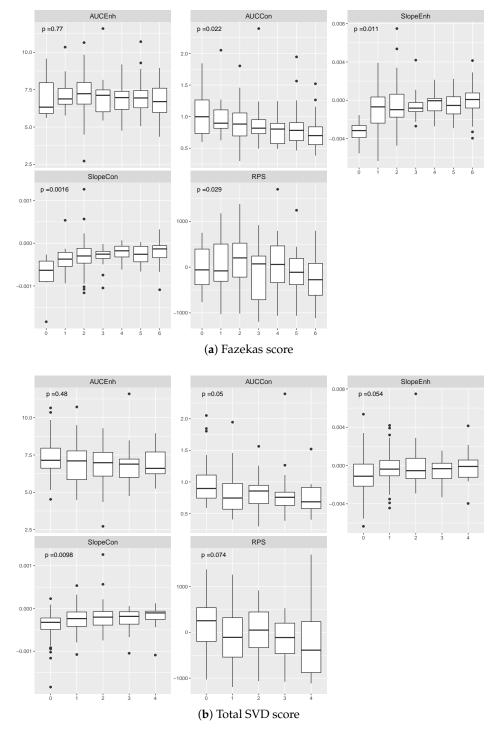## 2.4. Validation against Clinical Parameters

We considered one-way analysis of variance (ANOVA) to evaluate the considered measures of contrast uptake/washout against clinical visual assessments related to SVD severity (i.e., Fazekas and total SVD scores), and multiple linear regression to establish whether age, diabetes, stroke lesion subtype, WMH volume, and stroke lesion volume were associated with them, after adjusting for biological sex, mean arterial blood pressure, hyperlipidaemia, and smoking status. For ANOVA tests, we used the following notation: $(F(k - 1, n - k) = F\text{-value}, p, \eta^2, \omega^2)$, where k represents the number of groups (i.e., 7 and 5 for Fazekas and total SVD score, respectively), n the sample size, F-value the F test statistic, p the p-value, and η^2 and ω^2 are effect size estimators which indicate the proportion of data variance explained by predictors. For multiple linear regression, we reported β (95% CI) and p-value for each predictor, which indicate their weight in the model and whether the predictor is significant in the model, respectively. Also, we reported the adjusted R^2 values which specify the percentage of data variance in the outcome variable explained by predictors. We carried out our statistical analyses using RStudio v1.1.456 with R v3.5.1.

3. Results

3.1. Comparison of Effect Sizes

We evaluated the effect of the measures of contrast uptake/washout computed in cerebrospinal fluid and WMH against two relevant visual clinical ratings (Fazekas and SVD scores).
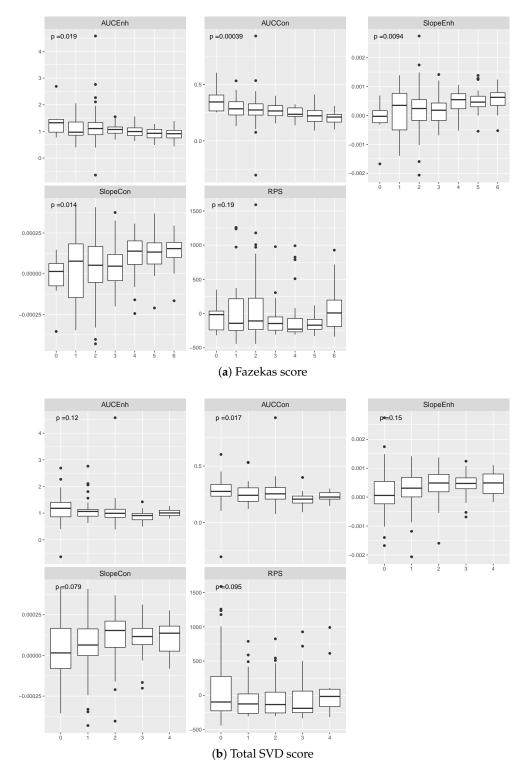
The effect of the burden of WMH on most vascular function measures computed from the cerebrospinal fluid regions was significant (AUC_{Con}: $F(6, 190) = 2.54$, $p < 0.05$, $\eta^2 = 7\%$, $\omega^2 = 5\%$; $Slope_{Enh}$: $F(6, 190) = 2.87$, $p < 0.05$, $\eta^2 = 8\%$, $\omega^2 = 5\%$; $Slope_{Con}$: $F(6, 190) = 3.71$, $p < 0.01$, $\eta^2 = 11\%$, $\omega^2 = 8\%$, RPS: $F(6, 190) = 2.40$, $p < 0.05$, $\eta^2 = 7\%$, $\omega^2 = 4\%$), except on the AUC_{Enh} (AUC_{Enh}: $F(6, 190) = 0.55$, $p > 0.10$, $\eta^2 = 2\%$, $\omega^2 = -1\%$), as shown in Figure 3. The higher the Fazekas score, the lower the AUCs and the rising the Slopes. The association was stronger (higher η^2 and ω^2) for the $Slope_{Con}$ than the other four measures. The total burden of neuroimaging features of SVD, given by the total SVD score, was associated with the AUC_{Con}, $Slope_{Enh}$, and $Slope_{Con}$ (AUC_{Con}: $F(4, 192) = 2.42$, $p = 0.05$, $\eta^2 = 5\%$, $\omega^2 = 3\%$; $Slope_{Enh}$: $F(4, 192) = 2.37$, $p = 0.05$, $\eta^2 = 5\%$, $\omega^2 = 3\%$; $Slope_{Con}$: $F(4, 192) = 3.43$, $p < 0.01$, $\eta^2 = 7\%$, $\omega^2 = 5\%$), but not with the other measurements (AUC_{Enh}: $F(4, 192) = 0.48$, $p > 0.1$, $\eta^2 = 2\%$, $\omega^2 = 0\%$; RPS: $F(4, 192) = 2.17$, $p > 0.05$, $\eta^2 = 4\%$, $\omega^2 = 2\%$). The higher the total SVD score, the lower the AUCs and RPS, the rising the Slopes.

(**a**) Fazekas score

(**b**) Total SVD score

Figure 3. Estimated contrast uptake/washout extracted from cerebrospinal fluid for patients grouped by their (**a**) Fazekas and (**b**) total SVD scores. We computed the p-values using the ANOVA test. Data points located outside of the whiskers of each boxplot correspond to outliers.

The impact of the burden of WMH on most measures of contrast uptake/washout from WMH was significant (AUC_{Enh}: $F(6, 190) = 2.61$, $p < 0.05$, $\eta^2 = 8\%$, $\omega^2 = 5\%$; AUC_{Con}: $F(6, 190) = 4.35$, $p < 0.001$, $\eta^2 = 12\%$, $\omega^2 = 9\%$; $Slope_{Enh}$: $F(6, 190) = 2.93$, $p < 0.01$, $\eta^2 = 9\%$, $\omega^2 = 6\%$; $Slope_{Con}$: $F(6, 190) = 2.73$, $p < 0.05$, $\eta^2 = 8\%$, $\omega^2 = 5\%$), except on the RPS (RPS: $F(6, 190) = 1.48$, $p > 0.10$, $\eta^2 = 5\%$, $\omega^2 = 1\%$), as depicted in Figure 4. The higher the Fazekas score, the lower the AUCs and the rising the Slopes. The association was stronger for the AUC_{Con} than the other four measures. The burden SVD features was only associated with the AUC_{Con} ($F(4, 192) = 3.09$, $p < 0.05$, $\eta^2 = 6\%$,

$\omega^2 = 4\%$), but not with the other measurements (AUC_{Enh}: $F(4, 192) = 1.86$, $p > 0.1$, $\eta^2 = 4\%$, $\omega^2 = 2\%$; $Slope_{Enh}$: $F(4, 192) = 1.71$, $p > 0.10$, $\eta^2 = 3\%$, $\omega^2 = 1\%$; $Slope_{Con}$: $F(4, 192) = 2.12$, $p > 0.05$, $\eta^2 = 4\%$, $\omega^2 = 2\%$; RPS: $F(4, 192) = 2.01$, $p > 0.05$, $\eta^2 = 4\%$, $\omega^2 = 2\%$). The higher the total SVD score, the lower the AUCs, the rising the Slopes.

(**a**) Fazekas score

(**b**) Total SVD score

Figure 4. Estimated contrast uptake/washout extracted from white matter hyperintensities for patients grouped by their (**a**) Fazekas and (**b**) total SVD scores. We computed the p-values using the ANOVA test. Data points located outside of the whiskers of each boxplot correspond to outliers.

3.2. Relationship between Contrast Uptake/Washout Measures and Clinical Variables

We carried out multiple linear regression to investigate whether age, diabetes, stroke lesion subtype, WMH volume, and stroke lesion volume were associated with semiquantitative measures of contrast uptake/washout, after adjusting for biological sex, mean arterial pressure, smoker, and hyperlipidaemia. Corresponding regression results are condensed in Tables 1 and A1.

Table 1. Adjusted R^2 and p-values of multiple linear regression with semiquantitative contrast uptake/washout estimates per region of interest as predicted variables and clinical parameters as predictors. This table is a simplified version of Table A1. Adjusted R^2 values are shown as percentages. Significant associations appear in bold. Stroke type: 0—cortical, 1—lacunar. ROI: region of interest. CI: confidence interval. CSF: cerebrospinal fluid. DGM: deep grey matter. NAWM: normal-appearing white matter. WMH: white matter hyperintensity. SL: stroke lesion. RPS: radial power spectrum.

ROI	Method	R^2	p-Value	Age	Diabetes	Stroke Type	WMH Volume	SL Volume
CSF	AUC_{Enh}	16	$\mathbf{2.17 \times 10^{-6}}$	$\mathbf{5.02 \times 10^{-7}}$	5.85×10^{-1}	7.88×10^{-1}	3.90×10^{-1}	1.61×10^{-1}
	AUC_{Con}	36	$\mathbf{4.44 \times 10^{-16}}$	$\mathbf{3.77 \times 10^{-15}}$	8.32×10^{-1}	7.35×10^{-1}	7.69×10^{-1}	9.61×10^{-1}
	$Slope_{Enh}$	10	$\mathbf{5.92 \times 10^{-4}}$	$\mathbf{1.12 \times 10^{-4}}$	1.56×10^{-1}	6.24×10^{-1}	1.55×10^{-1}	4.43×10^{-1}
	$Slope_{Con}$	33	$\mathbf{9.97 \times 10^{-15}}$	$\mathbf{2.46 \times 10^{-13}}$	2.19×10^{-1}	3.98×10^{-1}	4.76×10^{-1}	2.03×10^{-1}
	RPS	2	1.78×10^{-1}	8.97×10^{-1}	7.46×10^{-1}	7.10×10^{-1}	6.79×10^{-2}	3.64×10^{-1}
DGM	AUC_{Enh}	3	8.11×10^{-2}	2.97×10^{-1}	$\mathbf{2.75 \times 10^{-2}}$	4.51×10^{-1}	8.53×10^{-2}	1.12×10^{-1}
	AUC_{Con}	13	$\mathbf{6.20 \times 10^{-5}}$	$\mathbf{9.30 \times 10^{-6}}$	$\mathbf{7.47 \times 10^{-4}}$	6.04×10^{-1}	7.75×10^{-1}	8.18×10^{-1}
	$Slope_{Enh}$	3	9.77×10^{-2}	1.93×10^{-1}	6.31×10^{-1}	6.54×10^{-1}	3.97×10^{-1}	6.90×10^{-1}
	$Slope_{Con}$	8	$\mathbf{3.59 \times 10^{-3}}$	$\mathbf{1.55 \times 10^{-2}}$	3.23×10^{-1}	7.59×10^{-1}	1.20×10^{-1}	9.86×10^{-1}
	RPS	5	$\mathbf{3.33 \times 10^{-2}}$	4.89×10^{-1}	1.09×10^{-1}	8.24×10^{-1}	$\mathbf{7.05 \times 10^{-3}}$	4.57×10^{-1}
NAWM	AUC_{Enh}	3	1.27×10^{-1}	2.68×10^{-1}	6.64×10^{-1}	4.53×10^{-1}	$\mathbf{2.47 \times 10^{-2}}$	5.82×10^{-1}
	AUC_{Con}	6	$\mathbf{1.07 \times 10^{-2}}$	$\mathbf{1.03 \times 10^{-4}}$	1.83×10^{-1}	3.84×10^{-1}	6.17×10^{-1}	3.19×10^{-1}
	$Slope_{Enh}$	−1	5.94×10^{-1}	7.04×10^{-1}	9.14×10^{-1}	2.27×10^{-1}	2.55×10^{-1}	3.50×10^{-1}
	$Slope_{Con}$	2	1.43×10^{-1}	2.73×10^{-1}	5.44×10^{-1}	1.94×10^{-1}	1.08×10^{-1}	1.09×10^{-1}
	RPS	−2	8.53×10^{-1}	9.57×10^{-1}	8.11×10^{-1}	5.49×10^{-1}	8.13×10^{-1}	9.97×10^{-1}
WMH	AUC_{Enh}	13	$\mathbf{3.60 \times 10^{-5}}$	$\mathbf{2.04 \times 10^{-2}}$	$\mathbf{3.07 \times 10^{-3}}$	7.86×10^{-1}	$\mathbf{1.37 \times 10^{-3}}$	$\mathbf{1.93 \times 10^{-2}}$
	AUC_{Con}	25	$\mathbf{2.49 \times 10^{-10}}$	$\mathbf{3.38 \times 10^{-6}}$	$\mathbf{1.25 \times 10^{-3}}$	9.94×10^{-1}	$\mathbf{1.98 \times 10^{-4}}$	8.61×10^{-1}
	$Slope_{Enh}$	4	6.11×10^{-2}	4.59×10^{-1}	5.35×10^{-1}	2.79×10^{-1}	4.04×10^{-1}	1.21×10^{-1}
	$Slope_{Con}$	4	7.23×10^{-2}	6.88×10^{-2}	2.92×10^{-1}	3.00×10^{-1}	3.25×10^{-1}	7.95×10^{-1}
	RPS	−3	9.58×10^{-1}	4.82×10^{-1}	3.88×10^{-1}	4.72×10^{-1}	8.78×10^{-1}	6.12×10^{-1}
SL	AUC_{Enh}	33	$\mathbf{9.90 \times 10^{-10}}$	5.04×10^{-1}	$\mathbf{3.43 \times 10^{-5}}$	$\mathbf{1.52 \times 10^{-5}}$	1.07×10^{-1}	$\mathbf{8.69 \times 10^{-4}}$
	AUC_{Con}	28	$\mathbf{6.33 \times 10^{-8}}$	2.21×10^{-1}	$\mathbf{6.73 \times 10^{-8}}$	$\mathbf{1.92 \times 10^{-3}}$	7.88×10^{-2}	6.87×10^{-1}
	$Slope_{Enh}$	14	$\mathbf{6.30 \times 10^{-4}}$	6.69×10^{-1}	5.05×10^{-2}	6.02×10^{-2}	1.63×10^{-1}	$\mathbf{4.36 \times 10^{-4}}$
	$Slope_{Con}$	13	$\mathbf{1.02 \times 10^{-3}}$	3.41×10^{-1}	$\mathbf{1.28 \times 10^{-3}}$	$\mathbf{2.17 \times 10^{-2}}$	1.04×10^{-1}	7.06×10^{-2}
	RPS	4	$\mathbf{4.51 \times 10^{-2}}$	9.52×10^{-1}	6.26×10^{-1}	6.31×10^{-1}	$\mathbf{2.95 \times 10^{-2}}$	$\mathbf{1.34 \times 10^{-3}}$

In the cerebrospinal fluid region, four vascular function measures showed associations with clinical variables ($p < 0.001$), RPS did not ($p > 0.1$). The associations were stronger (lower p-value, higher coefficients of determination) when considering concentration-time curves instead of enhancement-time curves (AUC: $R^2_{Enh} = 16\%$ vs. $R^2_{Con} = 36\%$; Slope: $R^2_{Enh} = 10\%$ vs. $R^2_{Con} = 33\%$). Age was negatively associated the AUCs and Slopes in the CSF ($AUC_{Enh} : \beta = -4.27 \times 10^{-2}$ [95% CI $-5.89 \times 10^{-2}, -2.65 \times 10^{-2}$], $p < 0.001$; $AUC_{Con} : \beta = -1.52 \times 10^{-2}$ [95% CI $-1.87 \times 10^{-2}, -1.17 \times 10^{-2}$], $p < 0.001$; $Slope_{Enh} : \beta = -3.51 \times 10^{-5}$ [95% CI $-5.27 \times 10^{-5}, -1.76 \times 10^{-5}$], $p < 0.001$; $Slope_{Con} : \beta = -1.29 \times 10^{-5}$ [95% CI $-1.61 \times 10^{-5}, -9.66 \times 10^{-6}$], $p < 0.001$). Clinical parameters predicted most variance in AUC_{Con} values compared to the four other methods (Adjusted $R^2 : AUC_{Con} = 36\%$ vs. $Slope_{Con} = 33, RPS = 2\%, AUC_{Enh} = 16\%, Slope_{Enh} = 10\%$).

In the deep grey matter, $AUC_{Con}, Slope_{Con}$, and RPS showed associations with clinical variables. Age was a strong predictor was negatively associated with AUC_{Con} and $Slope_{Con}$ ($AUC_{Con} : \beta = -2.29 \times 10^{-3}$ [95% CI $-3.29 \times 10^{-3}, -1.30 \times 10^{-3}$], $p < 0.001$; $Slope_{Con} : \beta = -1.35 \times 10^{-6}$ [95% CI $-2.43 \times 10^{-6}, -2.59 \times 10^{-7}$], $p < 0.05$). A diagnosis of diabetes was associated with an increase in the AUC_{Con} ($AUC_{Con} : \beta = 5.37 \times 10^{-2}$ [95% CI $2.28 \times 10^{-2}, 8.46 \times 10^{-2}$], $p < 0.001$). WMH volume was negatively associated with the RPS ($RPS : \beta = -3.19 \times 10^3$ [95% CI $-5.51 \times 10^3, -8.81 \times 10^3$], $p < 0.01$). Clinical parameters predicted the variance in AUC_{Con} values the best

compared to other methods (Adjusted R^2 : $AUC_{Con} = 13\%$ vs. $Slope_{Con} = 8, RPS = 5\%, AUC_{Enh} = 3\%, Slope_{Enh} = 3\%$).

In normal-appearing white matter, clinical parameters were weakly or not associated with the five measures of vascular function (i.e. $0.01 < p < 0.05$ and $p > 0.1$, respectively) as they explained between 1% and 6% of their variability. Age predicted the AUC_{Con} significantly (AUC_{Con} : $\beta = -1.81 \times 10^{-3}$ [95% CI $- 2.70 \times 10^{-3}$, -9.08×10^{-4}], $p < 0.001$).

In WMH, clinical variables predicted 13% and 25% of the variance in AUC_{Enh} and AUC_{Con} ($p < 0.001$). Age, diabetes, and WMH volume were significantly and consistently associated with AUC_{Enh} and AUC_{Con} ($p < 0.05$ and $p < 0.01$, respectively). An increase in AUC_{Enh} and AUC_{Con} was associated with younger age (AUC_{Enh} : $\beta = -6.81 \times 10^{-3}$ [95% CI $- 1.26 \times 10^{-2}$, -1.07×10^{-3}], $p < 0.05$; AUC_{Con} : $\beta = -2.88 \times 10^{-3}$ [95% CI $- 4.07 \times 10^{-3}$, -1.69×10^{-3}], $p < 0.001$), diabetes diagnosis (AUC_{Enh} : $\beta = 2.72 \times 10^{-1}$ [95% CI 9.31×10^{-1}, 4.51×10^{-1}], $p < 0.01$; AUC_{Con} : $\beta = 6.13 \times 10^{-2}$ [95% CI 2.44×10^{-2}, 9.82×10^{-2}], $p < 0.01$), and less WMH volume (AUC_{Enh} : $\beta = -4.46$ [95% CI $- 7.17$, -1.75], $p < 0.01$; AUC_{Con} : $\beta = -1.08$ [95% CI $- 1.63$, -0.52], $p < 0.001$). Moreover, the stroke lesion volume was positively associated with the AUC_{Enh} (AUC_{Enh} : $\beta = 6.38$ [95% CI 1.05, 11.7], $p < 0.01$).

In stroke lesions, all vascular function measures were associated with clinical variables ($p < 0.05$). The associations between clinical parameters and AUC_{Enh} and AUC_{Con} were clearer compared to those of the rest ($28\% \leq R^2 \leq 33\%$ vs. $4\% \leq R^2 \leq 14\%$). Three variables strongly predicted the outcome variables for some of these models: diabetes, stroke lesion subtype, and stroke lesion volume. A diagnosis of diabetes was significantly associated with an increase in AUCs and Slopes (AUC_{Enh} : $\beta = 1.13$ [95% CI 0.61, 1.65], $p < 0.001$; AUC_{Con} : $\beta = 0.31$ [95% CI 0.20, 0.41], $p < 0.001$; $Slope_{Enh}$: $\beta = 6.85 \times 10^{-4}$ [95% CI $- 1.45 \times 10^{-6}$, 1.37×10^{-3}], $p = 0.05$; $Slope_{Con}$: $\beta = 2.60 \times 10^{-4}$ [95% CI 1.04×10^{-4}, 4.16×10^{-4}], $p < 0.01$), but not with RPS ($p > 0.1$). Cortical strokes had higher AUCs and $Slope_{Con}$ (AUC_{Enh} : $\beta = -0.83$ [95% CI $- 1.20$, -0.47], $p < 0.001$; AUC_{Con} : $\beta = -0.12$ [95% CI $- 0.19$, -0.05], $p < 0.01$; $Slope_{Con}$: $\beta = -1.29 \times 10^{-4}$ [95% CI $- 2.38 \times 10^{-4}$, -1.92×10^{-5}], $p < 0.05$). Stroke volume was associated with an increase in AUC_{Enh}, $Slope_{Enh}$, and RPS (AUC_{Enh} : $\beta = 2.41 \times 10^1$ [95% CI 1.01×10^1, 3.82×10^1], $p < 0.001$; $Slope_{Enh}$: $\beta = 3.37 \times 10^{-2}$ [95% CI 1.52×10^{-2}, 5.22×10^{-2}], $p < 0.001$; RPS : $\beta = 7.16 \times 10^3$ [95% CI 2.82×10^3, 1.15×10^4], $p < 0.01$).

4. Discussion

In this work, we compared the performance of five semiquantitative methods for analysing signal-time trajectories of Gadolinium-based contrast agent in reflecting small vessel disease burden within healthy and pathological intracranial brain regions. The five methods estimate and analyse the slopes and area under the enhancement-time and concentration-time curves and changes in the power spectrum of the contrast-enhancement signal over time.

The considered semiquantitative measurements assessing contrast uptake/washout provide different yet complementary information related to cerebrovascular dysfunction. First, the areas under the enhancement-time/concentration-time curves describe two processes that may cause signal change in tissue jointly: accumulation of contrast agent in the extravascular extracellular space due to blood–brain barrier leakage and total volume of blood. Since the former effect is expected to be subtle in small vessel disease, we expect these areas under the curves to reflect more total blood volume. In regions filled with cerebrospinal fluid, increases in areas under the curves could be caused by contrast agent leakage due to an impaired blood-cerebrospinal fluid barrier [1–3]. Second, the slopes of the enhancement-time/concentration-time curves describe the rate at which the contrast agent washes out of brain tissues. While a positive slope reflects uptake of contrast agent in tissue over time, a negative slope reflects contrast washout over time. The magnitude of such a change indicates the speed at which it happens: the higher the magnitude, the faster the change over time. Thus, the slower the washout rate, the more the contrast agent stays in tissue potentially due to its accumulation in the

extracellular extravascular space. In regions filled with cerebrospinal fluid, a slope different from zero may reveal impairment of the blood–CSF barrier. Third, the analysis of the radial power spectrum permits quantifying changes in frequencies over time cohort-wise [8]. A positive or negative value expresses distancing from the mean behaviour (described by each eigenfunction) cohort-wise.

We performed a one-way ANOVA to determine the effect of the burden of WMH and neuroimaging features of SVD, expressed in terms of the Fazekas and total SVD scores, on the five measures of contrast uptake/washout from CSF and WMH. Most effects were significant on measurements extracted from both CSF and WMH considering Fazekas scores. The only significant effects when considering the total SVD score were the slope of the concentration-time curve extracted from regions filled with CSF and the area under the concentration-time extracted from WMH. These results imply that most measurements vary depending on the overall burden of WMH in the brain, but only concentration-time measurements capture additional aspects of vascular dysfunction on univariate analyses. Moreover, the relationship between measurements and clinical visual scores was more evident (lower *p*-values) when extracted from concentration-time curves. Therefore, the analysis of concentration-time curves is more reliable than enhancement-time curves since the former includes adjustment for contrast agent relaxivities, imaging parameters, and relaxation times of each region of interest. The slopes and areas under the curves exhibited opposite trends: slopes increased with WMH and total SVD score, whilst areas decreased. Examination on larger datasets with more varied states of brain vascular and other pathologies is needed to more fully understand the factors influencing the measurement of these potentially valuable differential vascular dysfunction parameters.

We performed multiple linear regression to establish whether clinical parameters (age, biological sex, mean arterial pressure, hyperlipidaemia, smoker, diabetes, stroke lesion subtype, WMH and stroke lesion volume) determined the extent of enhancement in cerebrospinal fluid, deep grey matter, normal-appearing white matter, WMH, and stroke lesion. The strength of the associations were consistently higher when considering measurements from the concentration-time curves and not from the enhancement-time curves consistent with the literature [1,4–6,19–23]. This might imply that the use of imaging parameters to obtain these former trajectories provide better estimates of the contrast uptake/washout. While the analysis of the area under the concentration-time curve was explained the best by clinical parameters regardless of the region of interest, the analysis of the radial power spectrum did not identify associations as they were the weakest compared to the other four measurements. The presence of noise and signal drift in similar levels to the signal changes has been acknowledged previously [9,24]. The RPS, reflective of the cumulative effect of the whole frequency spectrum forming the signal, is a sensitive measure worth further evaluation for this purpose once appropriate noise filtering procedures have been applied.

Estimates of contrast agent update/washout in cerebrospinal fluid-filled spaces, deep grey matter, normal-appearing white matter, and WMH were negatively associated with age. Given that the total volume of blood decreases with age [25] and that leakage in small vessel disease is expected to be subtle [3], this outcome suggests that the enhancement in the capillaries might be overshadowing the enhancement due to leakage and, hence, the semiquantitative methods considered in this work examine vascular surface area, in accordance with previous research in the field [26]. In WMH regions, our results indicate that their enhancement decreases with the extent of demyelination and axonal damage [27], consistent with previous findings [28–30]. In deep grey matter, WMH, and stroke lesions, diabetes influenced the contrast uptake/washout estimates: higher values in diabetic vs. non-diabetic patients. This outcome suggests that diabetic patients may present a reduction in capillary density or a higher impairment of the blood–brain barrier. In both cases, this relationship agrees with previous studies in which both hyper- and hypo-glycemia have been associated with cerebrovascular alterations [31] and compromised the blood–brain barrier [32,33]. In stroke lesions, large cortical strokes exhibited the highest contrast uptake/washout estimates, much more evident in diabetic patients. Further research in these directions is needed to account for the interaction between the capillaries and the extracellular extravascular space and their contribution to the overall enhancement.

Future work should consider comparing more semiquantitative and quantitative approaches for analysing concentration-time curves and assessing their robustness against imaging artefacts as they compromise current assessments [3,9–11].

Conflicts of Interest: The authors declare no conflict of interest. The funders had no role in the design of the study; in the collection, analyses, or interpretation of data; in the writing of the manuscript, or in the decision to publish the results.

Abbreviations

The following abbreviations are used in this manuscript:

ANOVA	Analysis of variance
AUC	Area under the curve
AUC_{Con}	Area under the concentration-time curve
AUC_{Enh}	Area under the enhancement-time curve
CI	Confidence interval
CSF	Blood-brain barrier
DCE-MRI	Dynamic contrast-enhanced magnetic resonance imaging
DGM	Deep grey matter
MAP	Mean arterial pressure
MRI	Magnetic resonance imaging
NAWM	Normal-appearing white matter
WMH	White matter hyperintensity
RPS	Radial power spectrum
SL	Stroke lesion
$Slope_{Con}$	Slope of the concentration-time curve
$Slope_{Enh}$	Slope of the enhancement-time curve
SVD	Small vessel disease
TE	Echo time
TI	Inversion time
TR	Repetition time

Appendix A

Table A1. Multiple linear regression results with semiquantitative contrast uptake/washout estimates per region of interest as predicted variables and clinical parameters as predictors. Adjusted R^2 values are shown as percentages. Biological sex: 0—female, 1—male. Stroke type: 0—cortical, 1—lacunar. ROI: region of interest. MAP: mean arterial pressure. CI: confidence interval. CSF: cerebrospinal fluid. DGM: deep grey matter. NAWM: normal-appearing white matter. WMH: white matter hyperintensity. SL: stroke lesion. RPS: radial power spectrum.

ROI	Method	R^2	p-Value	Age β (95%CI)	p-Value	Biological Sex β (95%CI)	p-Value	MAP β (95%CI)	p-Value	Hyperlipidaemia β (95%CI)	p-Value	Smoker β (95%CI)	p-Value	Diabetes β (95%CI)	p-Value	Stroke Type β (95%CI)	p-Value	WMH Volume β (95%CI)	p-Value	SL Volume β (95%CI)	p-Value
CSF	AUC_{Enh}	16	2.17×10^{-6}	-4.27×10^{-2} (-5.89×10^{-2}, -2.65×10^{-2})	5.02×10^{-7}	-5.46×10^{-1} (-8.78×10^{-1}, -2.14×10^{-1})	1.40×10^{-3}	-4.41×10^{-3} (-1.53×10^{-2}, 6.48×10^{-3})	4.25×10^{-1}	-1.10×10^{-1} (-4.44×10^{-1}, 2.24×10^{-1})	5.17×10^{-1}	-9.63×10^{-2} (-4.42×10^{-1}, 2.50×10^{-1})	5.84×10^{-1}	-1.40×10^{-1} (-6.44×10^{-1}, 3.64×10^{-1})	5.85×10^{-1}	-4.65×10^{-2} (-3.88×10^{-1}, 2.95×10^{-1})	7.88×10^{-1}	3.33×10^{0} (-4.30×10^{0}, 1.10×10^{1})	3.90×10^{-1}	1.07×10^{1} (-4.32×10^{0}, 2.57×10^{1})	1.61×10^{-1}
	AUC_{Con}	36	4.44×10^{-16}	-1.52×10^{-2} (-1.87×10^{-2}, -1.17×10^{-2})	3.77×10^{-15}	-1.40×10^{-1} (-2.12×10^{-1}, -6.84×10^{-2})	1.61×10^{-4}	-9.58×10^{-4} (-3.31×10^{-3}, 1.39×10^{-3})	4.23×10^{-1}	-3.73×10^{-2} (-1.10×10^{-1}, 3.48×10^{-2})	3.09×10^{-1}	1.18×10^{-2} (-6.30×10^{-2}, 8.67×10^{-2})	7.56×10^{-1}	-1.17×10^{-2} (-1.21×10^{-1}, 9.72×10^{-2})	8.32×10^{-1}	-1.27×10^{-2} (-8.65×10^{-2}, 6.12×10^{-2})	7.35×10^{-1}	2.46×10^{-1} (-1.40×10^{0}, 1.89×10^{0})	7.69×10^{-1}	-8.12×10^{-1} (-3.33×10^{0}, 3.17×10^{0})	9.61×10^{-1}
	$Slope_{Enh}$	10	5.92×10^{-4}	-3.51×10^{-3} (-5.27×10^{-3}, -1.76×10^{-3})	1.12×10^{-4}	-1.50×10^{-2} (-5.10×10^{-2}, 2.11×10^{-2})	4.14×10^{-1}	-6.13×10^{-6} (-1.79×10^{-3}, 5.68×10^{-6})	3.07×10^{-1}	-1.98×10^{-2} (-3.82×10^{-4}, 3.42×10^{-4})	9.14×10^{-1}	-1.32×10^{-4} (-5.08×10^{-4}, 2.43×10^{-4})	4.88×10^{-1}	3.95×10^{-4} (-1.52×10^{-4}, 9.41×10^{-4})	1.56×10^{-1}	-9.23×10^{-5} (-4.63×10^{-4}, 2.78×10^{-4})	6.24×10^{-1}	-5.99×10^{-3} (-1.43×10^{-2}, 2.28×10^{-3})	1.55×10^{-1}	6.36×10^{-3} (-9.95×10^{-3}, 2.27×10^{-2})	4.43×10^{-1}
	$Slope_{Con}$	33	9.97×10^{-15}	-1.29×10^{-5} (-1.61×10^{-5}, -9.66×10^{-6})	2.46×10^{-3}	-1.19×10^{-4} (-1.85×10^{-4}, -5.27×10^{-5})	4.97×10^{-4}	-1.71×10^{-6} (-3.88×10^{-6}, 4.51×10^{-7})	1.20×10^{-1}	-3.71×10^{-6} (-7.01×10^{-5}, 6.27×10^{-5})	9.12×10^{-1}	1.58×10^{-5} (-5.08×10^{-4}, 3.47×10^{-5})	6.51×10^{-1}	6.27×10^{-5} (-3.76×10^{-5}, 1.63×10^{-4})	2.19×10^{-1}	-2.92×10^{-5} (-9.72×10^{-5}, 3.88×10^{-5})	3.98×10^{-1}	-5.49×10^{-4} (-2.07×10^{-3}, 9.68×10^{-4})	4.76×10^{-1}	1.94×10^{-3} (-1.05×10^{-3}, 4.93×10^{-3})	2.03×10^{-1}
	RPS	2	1.78×10^{-1}	-5.43×10^{-1} (-8.80×10^{0}, 7.71×10^{0})	8.97×10^{-1}	2.94×10^{1} (-1.40×10^{2}, 1.99×10^{2})	7.32×10^{-1}	-8.9×10^{-1} (-6.39×10^{0}, 4.71×10^{0})	7.66×10^{-1}	-2.16×10^{1} (-1.92×10^{2}, 1.49×10^{2})	8.02×10^{-1}	1.85×10^{1} (8.97×10^{0}, 3.62×10^{2})	3.95×10^{-2}	-4.23×10^{1} (-2.99×10^{2}, 2.15×10^{2})	7.46×10^{-1}	3.29×10^{1} (-1.41×10^{2}, 2.07×10^{2})	7.10×10^{-1}	-3.62×10^{0} (-7.50×10^{3}, 2.69×10^{2})	6.79×10^{-2}	-3.53×10^{3} (-1.12×10^{4}, 4.13×10^{3})	3.64×10^{-1}
DGM	AUC_{Enh}	3	8.11×10^{-2}	-2.55×10^{-3} (-7.37×10^{-3}, 2.26×10^{-3})	2.97×10^{-1}	3.37×10^{-2} (-6.51×10^{-2}, 1.33×10^{-1})	5.02×10^{-1}	-8.73×10^{-4} (-4.11×10^{-3}, 2.36×10^{-3})	5.95×10^{-1}	-2.97×10^{-2} (-1.29×10^{-1}, 6.96×10^{-2})	5.56×10^{-1}	-8.02×10^{-2} (-1.83×10^{-1}, 2.28×10^{-2})	1.26×10^{-1}	1.69×10^{-1} (1.89×10^{-2}, 3.19×10^{-1})	2.75×10^{-2}	3.89×10^{-2} (-6.27×10^{-2}, 1.41×10^{-1})	4.51×10^{-1}	1.99×10^{0} (-2.79×10^{-1}, 4.26×10^{0})	8.53×10^{-2}	3.62×10^{0} (-8.48×10^{-1}, 8.09×10^{0})	1.12×10^{-1}
	AUC_{Con}	13	6.20×10^{-5}	-2.29×10^{-3} (-3.29×10^{-3}, -1.30×10^{-3})	9.30×10^{-6}	-1.52×10^{-2} (-2.59×10^{-2}, 1.49×10^{-2})	5.94×10^{-1}	-8.96×10^{-3} (-7.57×10^{-4}, 5.78×10^{-4})	7.92×10^{-1}	-1.53×10^{-2} (-3.58×10^{-2}, 5.13×10^{-3})	4.32×10^{-1}	-7.05×10^{-3} (-2.83×10^{-2}, 1.42×10^{-2})	5.13×10^{-1}	5.37×10^{-2} (2.28×10^{-2}, 8.46×10^{-2})	7.47×10^{-4}	5.52×10^{-3} (-1.54×10^{-2}, 1.30×10^{-1})	6.04×10^{-1}	-6.77×10^{-2} (-5.35×10^{-1}, 4.00×10^{-1})	7.75×10^{-1}	-1.08×10^{-1} (-1.03×10^{0}, 8.14×10^{-1})	8.18×10^{-1}
	$Slope_{Enh}$	3	9.77×10^{-2}	-3.00×10^{-6} (-7.52×10^{-6}, 1.53×10^{-6})	1.93×10^{-1}	-1.27×10^{-4} (-2.20×10^{-4}, -3.39×10^{-5})	7.73×10^{-3}	-2.50×10^{-6} (-5.54×10^{-6}, 5.42×10^{-7})	1.07×10^{-1}	3.72×10^{-5} (-5.60×10^{-5}, 1.30×10^{-4})	4.32×10^{-1}	1.83×10^{-5} (-7.84×10^{-5}, 1.15×10^{-4})	7.09×10^{-1}	3.43×10^{-5} (-1.06×10^{-4}, 1.75×10^{-4})	6.31×10^{-1}	2.17×10^{-5} (-7.37×10^{-5}, 1.17×10^{-4})	6.54×10^{-1}	-9.17×10^{-4} (-3.05×10^{-3}, 1.21×10^{-3})	3.97×10^{-1}	8.51×10^{-4} (-3.35×10^{-3}, 5.05×10^{-3})	6.90×10^{-1}
	$Slope_{Con}$	8	3.59×10^{-3}	-1.35×10^{-6} (-2.43×10^{-6}, -2.59×10^{-7})	1.55×10^{-2}	-2.94×10^{-5} (-5.17×10^{-5}, -7.08×10^{-6})	1.01×10^{-2}	-4.97×10^{-7} (-1.23×10^{-6}, 2.33×10^{-7})	1.81×10^{-1}	7.61×10^{-6} (-1.48×10^{-5}, 3.00×10^{-5})	5.04×10^{-1}	9.31×10^{-6} (-1.39×10^{-5}, 3.25×10^{-5})	4.30×10^{-1}	1.70×10^{-5} (-1.68×10^{-5}, 5.08×10^{-5})	3.23×10^{-1}	3.57×10^{-6} (-1.94×10^{-5}, 2.65×10^{-5})	7.59×10^{-1}	-4.05×10^{-4} (-9.17×10^{-4}, 1.06×10^{-4})	1.20×10^{-1}	-8.70×10^{-4} (-1.02×10^{-3}, 1.00×10^{-3})	9.86×10^{-1}
	RPS	5	3.33×10^{-2}	2.36×10^{1} (-3.18×10^{0}, 6.64×10^{0})	4.89×10^{-1}	-6.55×10^{1} (-1.66×10^{2}, 3.53×10^{1})	2.02×10^{-1}	-2.14×10^{0} (-5.44×10^{0}, 1.16×10^{0})	2.03×10^{-1}	-2.09×10^{1} (-1.22×10^{2}, 8.04×10^{1})	6.84×10^{-1}	5.72×10^{1} (-4.78×10^{1}, 1.62×10^{2})	2.84×10^{-1}	-1.25×10^{1} (-2.77×10^{2}, 2.82×10^{1})	1.09×10^{-1}	1.17×10^{1} (-9.19×10^{1}, 1.15×10^{2})	8.24×10^{-1}	-3.19×10^{1} (-5.51×10^{3}, -8.81×10^{2})	7.05×10^{-1}	-1.72×10^{3} (-6.28×10^{3}, 2.84×10^{3})	4.57×10^{-1}
NAWM	AUC_{Enh}	3	1.27×10^{-1}	-1.58×10^{-3} (-4.38×10^{-3}, 1.23×10^{-3})	2.68×10^{-1}	-3.34×10^{-2} (-9.09×10^{-2}, 2.42×10^{-2})	2.54×10^{-1}	-5.93×10^{-4} (-2.48×10^{-3}, 1.29×10^{-3})	5.35×10^{-1}	-1.65×10^{-2} (-7.43×10^{-2}, 4.13×10^{-2})	5.74×10^{-1}	-6.89×10^{-2} (-1.29×10^{-1}, -8.95×10^{-3})	2.45×10^{-2}	1.92×10^{-2} (-6.80×10^{-2}, 2.06×10^{-1})	6.64×10^{-1}	-2.25×10^{-2} (-8.17×10^{-2}, 3.66×10^{-2})	4.53×10^{-1}	1.51×10^{0} (1.95×10^{-1}, 2.83×10^{0})	2.47×10^{-2}	7.27×10^{-1} (-1.88×10^{0}, 3.33×10^{0})	5.82×10^{-1}
	AUC_{Con}	6	1.07×10^{-2}	-1.81×10^{-3} (-2.70×10^{-3}, -9.08×10^{-4})	1.03×10^{-4}	-7.85×10^{-3} (-2.63×10^{-2}, 1.06×10^{-2})	4.02×10^{-1}	-9.61×10^{-3} (-6.50×10^{-4}, 5.56×10^{-4})	8.78×10^{-1}	-9.61×10^{-3} (-2.81×10^{-2}, 8.90×10^{-3})	3.07×10^{-1}	-1.48×10^{-2} (-3.40×10^{-2}, 4.38×10^{-3})	1.30×10^{-1}	1.89×10^{-2} (-8.99×10^{-2}, 4.69×10^{-2})	1.83×10^{-1}	-8.38×10^{-3} (-2.73×10^{-2}, 1.05×10^{-2})	3.84×10^{-1}	1.07×10^{-1} (-3.15×10^{-1}, 5.30×10^{-1})	6.17×10^{-1}	-4.22×10^{-1} (-1.25×10^{0}, 4.12×10^{-1})	3.19×10^{-1}
	$Slope_{Enh}$	−1	5.94×10^{-1}	6.78×10^{-7} (-2.84×10^{-6}, 4.19×10^{-6})	7.04×10^{-1}	-2.42×10^{-5} (-9.64×10^{-5}, 4.80×10^{-5})	5.09×10^{-1}	-1.43×10^{-8} (-2.38×10^{-6}, 2.35×10^{-6})	9.90×10^{-1}	6.60×10^{-6} (-6.48×10^{-6}, 1.39×10^{-4})	7.40×10^{-2}	2.84×10^{-5} (-4.68×10^{-5}, 1.04×10^{-4})	4.58×10^{-1}	-5.99×10^{-6} (-1.15×10^{-4}, 1.03×10^{-4})	9.14×10^{-1}	-4.56×10^{-5} (-1.20×10^{-4}, 2.87×10^{-5})	2.27×10^{-1}	-9.58×10^{-4} (-2.61×10^{-3}, 6.98×10^{-4})	2.55×10^{-1}	-1.55×10^{-3} (-4.81×10^{-3}, 1.72×10^{-3})	3.50×10^{-1}
	$Slope_{Con}$	2	1.43×10^{-1}	-6.60×10^{-7} (-1.84×10^{-6}, 5.23×10^{-7})	2.73×10^{-1}	-7.77×10^{-6} (-3.21×10^{-5}, 1.65×10^{-5})	5.29×10^{-1}	2.02×10^{-7} (-5.93×10^{-7}, 9.98×10^{-7})	6.16×10^{-1}	1.94×10^{-5} (-5.01×10^{-6}, 4.38×10^{-5})	1.19×10^{-1}	9.82×10^{-6} (-1.39×10^{-5}, 3.25×10^{-5})	4.45×10^{-1}	1.14×10^{-5} (-2.55×10^{-5}, 4.82×10^{-5})	5.44×10^{-1}	-1.65×10^{-5} (-4.15×10^{-5}, 8.48×10^{-6})	1.94×10^{-1}	-4.56×10^{-4} (-2.00×10^{-3}, 1.02×10^{-4})	1.08×10^{-1}	-8.97×10^{-4} (-2.00×10^{-3}, 2.01×10^{-4})	1.09×10^{-1}
	RPS	−2	8.53×10^{-1}	2.36×10^{1} (-8.40×10^{0}, 8.87×10^{0})	9.57×10^{-1}	1.59×10^{0} (-1.83×10^{0}, 3.36×10^{2})	7.85×10^{-2}	1.39×10^{-1} (-5.67×10^{0}, 5.94×10^{0})	9.62×10^{-1}	1.52×10^{0} (-1.63×10^{2}, 1.93×10^{2})	8.67×10^{-1}	9.35×10^{1} (-9.12×10^{1}, 2.78×10^{2})	3.19×10^{-1}	3.26×10^{1} (-2.36×10^{2}, 3.01×10^{2})	8.11×10^{-1}	5.55×10^{1} (-1.27×10^{2}, 2.38×10^{2})	5.49×10^{-1}	4.87×10^{2} (-3.58×10^{3}, 4.55×10^{3})	8.13×10^{-1}	-1.74×10^{1} (-8.04×10^{3}, 8.00×10^{3})	9.97×10^{-1}
WMH	AUC_{Enh}	13	3.60×10^{-3}	-6.81×10^{-3} (-1.26×10^{-2}, -1.07×10^{-3})	2.04×10^{-2}	5.37×10^{-2} (-6.42×10^{-2}, 1.72×10^{-1})	3.70×10^{-1}	2.29×10^{-4} (-3.63×10^{-3}, 4.09×10^{-3})	9.07×10^{-1}	-1.68×10^{-1} (-1.35×10^{-1}, 1.02×10^{-1})	7.80×10^{-1}	-1.73×10^{-2} (-1.40×10^{-1}, 1.06×10^{-1})	7.81×10^{-1}	2.72×10^{-1} (9.31×10^{-2}, 4.51×10^{-1})	3.07×10^{-3}	1.67×10^{-2} (-1.05×10^{-1}, 1.38×10^{-1})	7.86×10^{-1}	-4.46×10^{0} (-7.17×10^{0}, -1.75×10^{0})	1.37×10^{-3}	6.38×10^{0} (1.05×10^{0}, 1.17×10^{1})	1.93×10^{-2}
	AUC_{Con}	25	2.49×10^{-10}	-2.88×10^{-3} (-4.07×10^{-3}, -1.69×10^{-3})	3.38×10^{-6}	1.96×10^{-2} (-4.78×10^{-3}, 4.39×10^{-2})	1.15×10^{-1}	1.20×10^{-3} (-6.78×10^{-4}, 9.17×10^{-4})	7.67×10^{-1}	-4.53×10^{-2} (-3.75×10^{-2}, 1.14×10^{-2})	2.95×10^{-1}	-1.98×10^{-2} (-2.99×10^{-2}, 2.08×10^{-2})	7.25×10^{-1}	6.13×10^{-2} (2.44×10^{-2}, 9.82×10^{-2})	1.25×10^{-3}	-1.02×10^{-2} (-1.63×10^{0}, -5.17×10^{-1})	9.94×10^{-1}	-1.08×10^{1} (-1.63×10^{0}, 1.72×10^{-1})	1.98×10^{-2}	-9.75×10^{1} (-1.20×10^{0}, 1.00×10^{0})	8.61×10^{-1}
	$Slope_{Enh}$	4	6.11×10^{-2}	-2.23×10^{-6} (-8.17×10^{-6}, 3.70×10^{-6})	4.59×10^{-1}	-1.61×10^{-4} (-2.83×10^{-4}, -3.90×10^{-5})	9.94×10^{-3}	-1.01×10^{-6} (-5.00×10^{-6}, 2.98×10^{-6})	6.18×10^{-1}	1.11×10^{-4} (-1.12×10^{-5}, 2.34×10^{-4})	7.47×10^{-2}	8.52×10^{-5} (-4.18×10^{-5}, 2.12×10^{-4})	1.87×10^{-1}	5.82×10^{-5} (-1.27×10^{-4}, 2.43×10^{-4})	5.35×10^{-1}	-6.90×10^{-5} (-1.94×10^{-4}, 5.63×10^{-5})	2.79×10^{-1}	1.19×10^{-3} (-1.61×10^{-3}, 3.98×10^{-3})	4.04×10^{-1}	4.35×10^{-3} (-1.16×10^{-3}, 9.87×10^{-3})	1.21×10^{-1}
	$Slope_{Con}$	4	7.23×10^{-2}	-1.32×10^{-6} (-2.74×10^{-6}, 1.03×10^{-7})	6.88×10^{-2}	-3.76×10^{-5} (-6.68×10^{-5}, -8.43×10^{-6})	1.18×10^{-2}	-2.34×10^{-7} (-1.19×10^{-6}, 7.22×10^{-7})	6.30×10^{-1}	2.53×10^{-5} (-4.03×10^{-6}, 5.47×10^{-5})	9.04×10^{-2}	2.05×10^{-5} (-1.02×10^{-5}, 5.07×10^{-5})	1.91×10^{-1}	2.37×10^{-5} (-2.06×10^{-5}, 6.80×10^{-3})	2.92×10^{-1}	-1.58×10^{-5} (-4.58×10^{-5}, 1.42×10^{-5})	3.00×10^{-1}	3.35×10^{-4} (-3.35×10^{-4}, 1.00×10^{-3})	3.25×10^{-1}	1.74×10^{-3} (-1.15×10^{-3}, 1.50×10^{-3})	7.95×10^{-1}
	RPS	−3	9.58×10^{-1}	1.90×10^{0} (-3.43×10^{0}, 7.23×10^{0})	4.82×10^{-1}	5.00×10^{1} (-5.94×10^{1}, 1.59×10^{2})	3.68×10^{-1}	9.04×10^{-1} (-2.68×10^{0}, 4.49×10^{0})	6.19×10^{-1}	-2.76×10^{1} (-1.37×10^{2}, 8.23×10^{1})	6.21×10^{-1}	1.13×10^{1} (-1.03×10^{2}, 1.25×10^{2})	8.45×10^{-1}	-7.28×10^{1} (-2.39×10^{2}, 9.31×10^{1})	3.88×10^{-1}	-4.11×10^{1} (-1.54×10^{2}, 7.14×10^{1})	4.72×10^{-1}	1.96×10^{2} (-2.31×10^{3}, 2.71×10^{3})	8.78×10^{-1}	-1.27×10^{3} (-6.22×10^{3}, 3.67×10^{3})	6.12×10^{-1}
SL	AUC_{Enh}	33	9.90×10^{-10}	5.95×10^{-3} (-1.16×10^{-2}, 2.35×10^{-2})	5.04×10^{-1}	2.28×10^{-1} (-1.27×10^{-1}, 5.83×10^{-1})	2.06×10^{-1}	2.36×10^{-3} (-9.03×10^{-3}, 1.38×10^{-2})	6.82×10^{-1}	2.18×10^{-1} (-1.28×10^{-1}, 5.65×10^{-1})	2.15×10^{-1}	1.40×10^{0} (-2.16×10^{-1}, 4.96×10^{-1})	4.38×10^{-1}	1.13×10^{0} (6.10×10^{-1}, 1.65×10^{0})	3.43×10^{-5}	-8.31×10^{-1} (-1.48×10^{0}, 1.45×10^{0})	1.52×10^{-5}	1.99×10^{0} (-1.48×10^{0}, 1.45×10^{0})	1.07×10^{-1}	2.41×10^{1} (1.01×10^{0}, 3.82×10^{1})	8.69×10^{-4}
	AUC_{Con}	28	6.33×10^{-8}	-2.22×10^{-3} (-5.78×10^{-3}, 1.35×10^{-3})	2.21×10^{-1}	5.17×10^{-2} (-2.02×10^{-2}, 1.24×10^{-1})	1.58×10^{-1}	6.43×10^{-3} (-1.67×10^{-2}, 2.95×10^{-3})	5.82×10^{-1}	3.20×10^{-2} (-3.83×10^{-2}, 1.02×10^{-1})	3.70×10^{-1}	1.98×10^{-2} (-5.23×10^{-2}, 9.20×10^{-2})	5.88×10^{-1}	3.06×10^{-1} (2.00×10^{-1}, 4.11×10^{-1})	6.73×10^{-8}	-1.19×10^{-1} (-1.93×10^{-1}, -4.45×10^{-2})	1.92×10^{-5}	1.07×10^{0} (-3.11×10^{0}, 5.47×10^{0})	7.88×10^{-1}	2.63×10^{0} (-2.05×10^{-1}, 5.47×10^{0})	6.87×10^{-1}
	$Slope_{Enh}$	14	6.30×10^{-4}	5.02×10^{-6} (-1.81×10^{-6}, 2.82×10^{-5})	6.69×10^{-1}	1.69×10^{-4} (-2.99×10^{-4}, 6.37×10^{-4})	4.77×10^{-1}	2.74×10^{-6} (-1.23×10^{-5}, 1.78×10^{-5})	7.19×10^{-1}	1.45×10^{-4} (-3.12×10^{-4}, 6.03×10^{-4})	5.30×10^{-1}	2.41×10^{-4} (-2.28×10^{-4}, 7.10×10^{-4})	3.12×10^{-1}	6.85×10^{-4} (-1.45×10^{-6}, 1.37×10^{-3})	5.05×10^{-2}	-4.62×10^{-4} (-9.44×10^{-4}, 2.01×10^{-5})	6.02×10^{-2}	-7.57×10^{-3} (-1.61×10^{-2}, 5.70×10^{-3})	1.63×10^{-1}	3.37×10^{-2} (1.52×10^{-2}, 5.22×10^{-2})	4.36×10^{-4}
	$Slope_{Con}$	13	1.02×10^{-3}	-2.54×10^{-6} (-7.81×10^{-6}, 2.73×10^{-6})	3.41×10^{-1}	5.33×10^{-5} (-5.32×10^{-5}, 1.60×10^{-4})	3.24×10^{-1}	1.43×10^{-6} (-1.98×10^{-6}, 4.85×10^{-6})	4.08×10^{-1}	3.69×10^{-5} (-6.71×10^{-5}, 1.41×10^{-4})	4.84×10^{-1}	8.71×10^{-5} (-9.81×10^{-6}, 1.15×10^{-4})	8.72×10^{-1}	2.60×10^{-4} (1.04×10^{-4}, 4.16×10^{-4})	1.28×10^{-3}	-1.29×10^{-4} (-2.38×10^{-4}, -1.92×10^{-5})	2.17×10^{-2}	-2.01×10^{-3} (-4.44×10^{-3}, 4.20×10^{-4})	1.04×10^{-1}	3.87×10^{-3} (-3.30×10^{-4}, 8.07×10^{-3})	7.06×10^{-2}
	RPS	4	4.51×10^{-2}	1.43×10^{-1} (-4.53×10^{0}, 4.81×10^{0})	9.52×10^{-1}	3.15×10^{1} (-6.44×10^{1}, 1.27×10^{2})	5.18×10^{-1}	5.64×10^{-1} (-2.58×10^{0}, 3.70×10^{0})	7.23×10^{-1}	-2.27×10^{1} (-1.19×10^{2}, 7.36×10^{1})	6.42×10^{-1}	1.45×10^{1} (-8.54×10^{1}, 1.14×10^{2})	7.75×10^{-1}	-3.59×10^{1} (-1.81×10^{2}, 1.09×10^{2})	6.26×10^{-1}	2.40×10^{1} (-7.46×10^{1}, 1.23×10^{2})	6.31×10^{-1}	2.45×10^{3} (2.46×10^{2}, 4.65×10^{3})	2.95×10^{-1}	7.16×10^{3} (2.82×10^{3}, 1.15×10^{4})	1.34×10^{-3}

References

1. Wardlaw, J.M.; Doubal, F.; Armitage, P.; Chappell, F.; Carpenter, T.; Muñoz Maniega, S.; Farrall, A.; Sudlow, C.; Dennis, M.; Dhillon, B. Lacunar stroke is associated with diffuse blood–brain barrier dysfunction. *Ann. Neurol.* **2009**, *65*, 194–202. [CrossRef]

2. Kidwell, C.; Burgess, R.; Menon, R.; Warach, S.; Latour, L. Hyperacute injury marker (HARM) in primary hemorrhage: A distinct form of CNS barrier disruption. *Neurology* **2011**, *77*, 1725–1728. [CrossRef] [PubMed]

3. Thrippleton, M.J.; Backes, W.H.; Sourbron, S.; Ingrisch, M.; van Osch, M.J.; Dichgans, M.; Fazekas, F.; Ropele, S.; Frayne, R.; van Oostenbrugge, R.J.; et al. Quantifying blood–brain barrier leakage in small vessel disease: Review and consensus recommendations. *Alzheimer's Dement.* **2019**, *15*, 840–858. [CrossRef] [PubMed]

4. Topakian, R.; Barrick, T.; Howe, F.; Markus, H. Blood–brain barrier permeability is increased in normal-appearing white matter in patients with lacunar stroke and leucoaraiosis. *J. Neurol. Neurosurg. Psychiatry* **2010**, *81*, 192–197. [CrossRef] [PubMed]

5. Muñoz Maniega, S.; Chappell, F.M.; Valdés Hernández, M.C.; Armitage, P.A.; Makin, S.D.; Heye, A.K.; Thrippleton, M.J.; Sakka, E.; Shuler, K.; Dennis, M.S.; et al. Integrity of normal-appearing white matter: Influence of age, visible lesion burden and hypertension in patients with small-vessel disease. *J. Cereb. Blood Flow Metab.* **2017**, *37*, 644–656. [CrossRef] [PubMed]

6. Wardlaw, J.M.; Makin, S.J.; Valdés-Hernández, M.C.; Armitage, P.A.; Heye, A.K.; Chappell, F.M.; Munoz-Maniega, S.; Sakka, E.; Shuler, K.; Dennis, M.S.; et al. Blood-brain barrier failure as a core mechanism in cerebral small vessel disease and dementia: Evidence from a cohort study. *Alzheimer's Dement.* **2017**, *13*, 634–643. [CrossRef]

7. Bernal, J.; Valdés-Hernández, M.d.C.; Escudero, J.; Armitage, P.A.; Makin, S.; Touyz, R.M.; Wardlaw, J.M. Analysis of spatial spectral features of dynamic contrast-enhanced brain magnetic resonance images for studying small vessel disease. In Proceedings of the Annual Conference on Medical Image Understanding and Analysis, Liverpool, UK, 24–26 July 2019; pp. 282–293.

8. Bernal, J.; Valdés-Hernández, M.d.C.; Escudero, J.; Viksne, L.; Heye, A.K.; Armitage, P.A.; Makin, S.; Touyz, R.M.; Wardlaw, J.M. Analysis of dynamic texture and spatial spectral descriptors of dynamic contrast-enhanced brain magnetic resonance images for studying small vessel disease. *Magn. Reson. Imaging* **2020**, *66*, 240–247. [CrossRef]

9. Armitage, P.A.; Farrall, A.J.; Carpenter, T.K.; Doubal, F.N.; Wardlaw, J.M. Use of dynamic contrast-enhanced MRI to measure subtle blood–brain barrier abnormalities. *Magn. Reson. Imaging* **2011**, *29*, 305–314. [CrossRef]

10. Barnes, S.R.; Ng, T.S.C.; Montagne, A.; Law, M.; Zlokovic, B.V.; Jacobs, R.E. Optimal acquisition and modeling parameters for accurate assessment of low Ktrans blood–brain barrier permeability using dynamic contrast-enhanced MRI. *Magn. Reson. Med.* **2016**, *75*, 1967–1977. [CrossRef]

11. Heye, A.K.; Thrippleton, M.J.; Armitage, P.A.; Valdés-Hernández, M.d.C.; Makin, S.D.; Glatz, A.; Sakka, E.; Wardlaw, J.M. Tracer kinetic modelling for DCE-MRI quantification of subtle blood–brain barrier permeability. *Neuroimage* **2016**, *125*, 446–455. [CrossRef]

12. Valdés-Hernández, M.d.C.; Armitage, P.A.; Thrippleton, M.J.; Chappell, F.; Sandeman, E.; Muñoz Maniega, S.; Shuler, K.; Wardlaw, J.M. Rationale, design and methodology of the image analysis protocol for studies of patients with cerebral small vessel disease and mild stroke. *Brain Behav.* **2015**, *5*, e00415. [CrossRef] [PubMed]

13. Wardlaw, J.M.; Chappell, F.M.; Valdés-Hernández, M.d.C.; Makin, S.D.; Staals, J.; Shuler, K.; Thrippleton, M.J.; Armitage, P.A.; Muñoz-Maniega, S.; Heye, A.K.; et al. White matter hyperintensity reduction and outcomes after minor stroke. *Neurology* **2017**, *89*, 1003–1010. [CrossRef] [PubMed]

14. Fazekas, F.; Niederkorn, K.; Schmidt, R.; Offenbacher, H.; Horner, S.; Bertha, G.; Lechner, H. White matter signal abnormalities in normal individuals: Correlation with carotid ultrasonography, cerebral blood flow measurements, and cerebrovascular risk factors. *Stroke* **1988**, *19*, 1285–1288. [CrossRef]

15. Staals, J.; Makin, S.D.; Doubal, F.N.; Dennis, M.S.; Wardlaw, J.M. Stroke subtype, vascular risk factors, and total MRI brain small-vessel disease burden. *Neurology* **2014**, *83*, 1228–1234. [CrossRef]

16. Valdés-Hernández, M.d.C.; Ferguson, K.J.; Chappell, F.M.; Wardlaw, J.M. New multispectral MRI data fusion technique for white matter lesion segmentation: Method and comparison with thresholding in FLAIR images. *Eur. Radiol.* **2010**, *20*, 1684–1691. [CrossRef] [PubMed]

17. Chapter 3 Power spectrum and its applications. In *Analysis of Geophysical Potential Fields*; Naidu, P.S.; Mathew, M., Eds.; Elsevier: Amsterdam, The Netherlands, 1998; Volume 5, pp. 75 – 143.

18. Happ, C.; Greven, S. Multivariate functional principal component analysis for data observed on different (dimensional) domains. *J. Am. Stat. Assoc.* **2018**, 1–11. [CrossRef]

19. Bronge, L.; Wahlund, L.O. White matter lesions in dementia: An MRI study on blood-brain barrier dysfunction. *Dement. Geriatr. Cogn. Disord.* **2000**, *11*, 263–267. [CrossRef] [PubMed]

20. Hanyu, H.; Asano, T.; Tanaka, Y.; Iwamoto, T.; Takasaki, M.; Abe, K. Increased blood-brain barrier permeability in white matter lesions of Binswanger's disease evaluated by contrast-enhanced MRI. *Dement. Geriatr. Cogn. Disord.* **2002**, *14*, 1–6. [CrossRef]

21. Wardlaw, J.M.; Farrall, A.; Armitage, P.A.; Carpenter, T.; Chappell, F.; Doubal, F.; Chowdhury, D.; Cvoro, V.; Dennis, M.S. Changes in background blood–brain barrier integrity between lacunar and cortical ischemic stroke subtypes. *Stroke* **2008**, *39*, 1327–1332. [CrossRef]

22. Wardlaw, J.M.; Doubal, F.N.; Valdes-Hernandez, M.; Wang, X.; Chappell, F.M.; Shuler, K.; Armitage, P.A.; Carpenter, T.C.; Dennis, M.S. Blood–brain barrier permeability and long-term clinical and imaging outcomes in cerebral small vessel disease. *Stroke* **2013**, *44*, 525–527. [CrossRef]

23. Starr, J.M.; Farrall, A.J.; Armitage, P.; McGurn, B.; Wardlaw, J. Blood–brain barrier permeability in Alzheimer's disease: A case–control MRI study. *Psychiatry Res. Neuroimaging* **2009**, *171*, 232–241. [CrossRef]

24. Heye, A.K.; Culling, R.D.; Valdés-Hernández, M.d.C.; Thrippleton, M.J.; Wardlaw, J.M. Assessment of blood–brain barrier disruption using dynamic contrast-enhanced MRI. A systematic review. *NeuroImage Clin.* **2014**, *6*, 262–274. [CrossRef] [PubMed]

25. Brown, W.R.; Thore, C.R. Cerebral microvascular pathology in ageing and neurodegeneration. *Neuropathol. Appl. Neurobiol.* **2011**, *37*, 56–74. [CrossRef] [PubMed]

26. Heye, A.K. Measurement of Subtle Blood-Brain Barrier Disruption in Cerebral Small Vessel Disease Using Dynamic Contrast-Enhanced Magnetic Resonance Imaging. Ph.D. Thesis, The University of Edinburgh, Edinburgh, UK, 2015.

27. Wardlaw, J.M.; Valdés-Hernández, M.C.; Muñoz-Maniega, S. What are white matter hyperintensities made of? Relevance to vascular cognitive impairment. *J. Am. Heart Assoc.* **2015**, *4*, e001140. [CrossRef] [PubMed]

28. Shi, Y.; Thrippleton, M.J.; Makin, S.D.; Marshall, I.; Geerlings, M.I.; de Craen, A.J.; van Buchem, M.A.; Wardlaw, J.M. Cerebral blood flow in small vessel disease: A systematic review and meta-analysis. *J. Cereb. Blood Flow Metab.* **2016**, *36*, 1653–1667. [CrossRef]

29. Bahrani, A.A.; Powell, D.K.; Yu, G.; Johnson, E.S.; Jicha, G.A.; Smith, C.D. White matter hyperintensity associations with cerebral blood flow in elderly subjects stratified by cerebrovascular risk. *J. Stroke Cerebrovasc. Dis.* **2017**, *26*, 779–786. [CrossRef]

30. Blair, G.W.; Thrippleton, M.J.; Shi, Y.; Hamilton, I.; Stringer, M.; Chappell, F.M.; Dickie, D.A.; Andrews, P.J.; Marshall, I.; Doubal, F.N.; et al. Intracranial functional haemodynamic relationships in patients with cerebral small vessel disease. *bioRxiv* **2019**. [CrossRef]

31. Biessels, G.J. Cerebral complications of diabetes: Clinical findings and pathogenetic mechanisms. *Neth. J. Med.* **1999**, *54*, 35–45. [CrossRef]

32. Prasad, S.; Sajja, R.K.; Naik, P.; Cucullo, L. Diabetes mellitus and blood-brain barrier dysfunction: An overview. *J. Pharmacovigil.* **2014**, *2*, 125.

33. Xu, R.S. Pathogenesis of diabetic cerebral vascular disease complication. *World J. Diabetes* **2015**, *6*, 54. [CrossRef] [PubMed]